3.1 Introduction

The development of new techniques in physics, biology, materials science, and chemistry, along with cutting-edge, possibly disruptive technologies, has allowed the field of chemical sensing to expand indefinitely. The motto of our research is to move away from lavish complex instrumentation to cheaper methods that can be activated by anyone e.g. the home pregnancy tests and glucose meter, which have gratified many in society [Swager et al., 2019]. Glutathione (GSH) plays a crucial role as an antioxidant through protective reactive oxygen species scavenging and cellular detoxification and also acts as a crucial arbitrator in numerous biological functions such as biothiol [Wu et al., 2019; Xianyu et al., 2015; Ni et al., 2015]. It is an important antioxidant that is produced endogenously and its irregular level in biological fluids is firmly associated with different diseases, like the aging of cells and cancers [Fruehauf et al., 2007; Tan et al., 2018]. As per the literature survey, the GSH level is higher in typical cancer cells [Perry et al., 1993; Fu et al., 2015; ko et al., 2014; Guo et al., 2012; Emoto et al., 2017]. Hence, the elevation of GSH concentration in cancer cells over healthy cells level is observed as a relevant physiological criterion for cancer detection and its diagnosis.

A cost-effective, reliable, fast response and efficient detection method for the quantification of cellular GSH levels is thus crucial for cancer cell recognition with various applications in the area of biomedical sciences. To date, various analytical techniques comprising electrochemistry [Wang et al., 2007; Liu et al., 2018; Wang et al 2008], high-performance liquid chromatography [Zhu et al., 2015; Yuan et al., 2011], spectrophotometry [Tcherkas et al., 2001; Rahman et al., 2007; Qiu et al., 2015], and fluorescent techniques [Zheng et al., 2015; Niu et al., 2015; Ni et al., 2018; Zhang et al., 2017; Zhang et al., 2020], are used for the quantification of GSH in biological samples. Since these methods bear limitations, such as tedious laboratory operations, expensive

instruments, and complex synthetic protocols, which are adverse for the practical applications [Shi et al., 2011]. Nowadays, the colorimetry method has drawn much attention because of its lower cost, higher sensitivity with lesser response time than other typical methods. This method allows naked eye onsite detection of analyte without involving any sophisticated instrumentation with good reproducibility [Nirala et al., 2017; Ojha et al., 2020] Horseradish Peroxidase (HRP) is a natural peroxidase enzyme that produces hydroxyl ($OH^{\cdot}$) radicals from H_2O_2. This $OH^{\cdot}$ radical, further, can be utilized to oxidize the chromogenic peroxidase substrate furnishing visual blue color contrasts in a colorimetric assay. HRP bears severe limitations as a due cause of its extreme intolerance to variations in environmental factors and cost involvement in isolation of the natural enzyme. To remove these constraints, HRP is being replaced by nanomaterials that have similar catalytic activity with higher stability over a long range of pH and temperature with lesser production cost. Some nanomaterials such as AuNP@MoS_2QDs [Vinita et al., 2018], GO-AuNC hybrid [Wen et al., 2014], Au-Pd bimetallic nanocomposite [Yang et al., 2016], Fe_3O_4-AuNPs [Tan et al., 2017], Ag@SiO_2 NPs [Lin et al., 2018], have been reported in the literature with remarkable peroxidase mimetic behaviour for the sensing of the wide varieties of the biomolecules utilizing the colorimetric assay. The significant loss of noble metals in a disposable way, high cost, and their uncontrolled aggregation limit their practical applications. Recently 2D materials have attained great privilege towards application in the field of nanozyme. MoS_2 categorizes typical two-dimensional transition metal dichalcogenides, which have found wide applications in the field of electronic devices, electrochemical sensors, catalysis, and energy storage owing to its natural abundance, large surface area, low toxicity, and easy surface modification. In the field of colorimetric sensors, different nanostructures like MoS_2 nanosheet, MoS_2 QDs have been applied for the sensing of biomolecules like glucose, choline, cysteine, etc. Hydrothermal

synthesis of these nanostructures bears exceptional advantages over chemical methods in regard to their precise control, high yield, uniform product, and ease of handling [Arul et al., 2016; Wang et al., 2014; Gu et al., 2016; Sun et al., 2020]. So, we have synthesized two-dimensional (2-D) nanomaterials, i.e., transition metal dichalcogenide MoS_2, using a hydrothermal method that has a huge surface area with good flexibility and control over morphology in the synthesis that provides unique properties and high substrate specificity for nanozymes [Zhao et al., 2015]. MoS_2 possesses intrinsic peroxidase activity and further to study the doping effect over its catalytic, it is doped with different transition non-noble metals ions (Fe, Ni, Co). It is found that Fe-doped MoS_2 (Fe-MoS_2) exhibited boost in the catalytic activity over other metal ions due to synergistic effect and in order to study the effect of percentage doping, different percentage of iron is doped (i.e. 0, 2.5, 5, 7.5, 10%) and its peroxidase activity has been tested. It has been observed that there is a synergistic enhancement in the peroxidase mimetic activity of Fe-MoS_2 with percentage doping reaching a saturation level at 10%. This remarkable mimetic activity of Fe-MoS_2 has been exploited for GSH detection using its inhibitory effect over peroxidase mimetic activity for the oxidation of TMB (3,3′,5,5′-tetramethylbenzidine) and results in the production of blue color contrast. Fe-MoS_2 showed excellent selectivity towards GSH in the range of 1-30 μM with a detection limit of 0.577μM at pH 4. In practical application, we hope that the developed method has good significance for the rapid and precise detection of GSH in serum material which may aid in the early diagnosis and treatment of several lethal diseases like cancer, aging, and heart problems.

3.2 Experimental section

3.2.1 Materials and Chemicals

Analytical grade chemicals are bought from commercial sources eg. Glutathione (GSH), 3,3′,5,5′-tetramethylbenzidine (TMB), 30% hydrogen peroxide, Ammonium molybdate ($(NH_4)_6Mo_7O_{24}\cdot 4H_2O$, horseradish peroxidase (HRP) was bought from SDFCL (≥ 99% purity, Product code-20028). Thiourea, Hydrochloric acid (HCl), Iron nitrate, Nickel nitrate, Cobalt nitrate, NaH_2PO_4 (sodium dihydrogen phosphate) and Na_2HPO_4 (disodium hydrogen phosphate) were purchased from Merck (Merck, India). Amino acids including L-glycine (Gly), L-alanine (Ala), L-aspartic acid (Asp), L-methionine (Met), L-glutamic acid (Glu), L-lysine (Lys), L-proline (Pro), L-tryptophane (Try), histidine (His) and L-serine (Ser) were all bought from CDH Fine Chemicals India. Sodium acetate anhydrous, and glacial acetic acid were obtained from Merck, India. The different ratios of Sodium acetate and acetic acid solutions were mixed to maintain the pH of the solution. Millipore water (18.02 Mcm^{-1}) was used for preparing all aqueous solutions. The blood serum samples for the GSH determination were collected from University hospital "the Institute of Medical Sciences, Banaras Hindu University" (courtesy Prof. D. Dash, IMS, BHU, Varanasi).

3.2.2 Apparatus and measurements

MoS_2 was synthesized in a 25 ml Teflon-lined hydrothermal reactor. Scanning Electron Microscopy (SEM) and Transmission Electron Microscopy (TEM) are used for morphological study. For elemental analysis X-ray photoelectron spectroscopy was performed (equipped with MgK_α (1.254 Å) radiation; Kratos analytical instrument; Shimadzu, Amicus XPS, UK). Powder X-Ray diffraction (XRD) was recorded by a Rigaku Miniflex 600 X-ray-diffractometer. Further absorption spectra are recorded to

study enzyme mimetic activity of Fe-MoS_2 using UV-Vis spectrophotometer (UV-2600, Shimadzu).

3.2.3 Synthesis of Fe-MoS_2, Co-MoS_2 and Ni-MoS_2

A facile and extensible hydrothermal method is required to synthesize Fe-MoS_2. 0.141g $Fe(NO_3)_3 \cdot 9H_2O$ was added in 18 mL of water with constant stirring followed by the addition of 1.14g of thiourea and 0.555g of $(NH_4)_6Mo_7O_{24} \cdot 4H_2O$ sequentially into the iron nitrate solution and continued stirring for 30 minutes. The reaction materials (Iron nitrate + Thiourea + Ammonium molybdate) were transferred into a Teflon autoclave to perform hydrothermal reaction. The Teflon vessel was tightened sealed and kept at 200°C for 24 hours in a vacuum oven before it was brought to room temperature. The black color precipitate was obtained and washing was done with distilled water several times until neutralization followed by ethanol and then dried at 60 °C in vacuum oven [Massey et al., 2016]. Similarly, Co-MoS_2 and Ni-MoS_2 were synthesized by using thiourea, $(NH_4)_6Mo_7O_{24} \cdot 4H_2O$ and cobalt nitrate, nickel nitrate respectively.

3.2.4 Colorimetric sensing of GSH using peroxidase mimetic activity of Co-MoS_2 and Ni-MoS_2 and Fe-MoS_2

500 mM solution of GSH (stock solution) was made in Millipore water and by sequential dilution of the stock solution, different GSH concentrations were obtained. For colorimetric sensing of GSH, 100µl of acetate buffer was poured into Eppendorf, then 50 µl of TMB (600µM), 100 µl of GSH having different concentration, 50µl of H_2O_2 (400µM) and 10µl of Fe-MoS_2 (0.2 µg/ml) were added sequentially to the above solution and kept at room temperature (RT) for 20 min. To elucidate the selectivity of the proposed method, 100 µl of different α-amino acids including Tyr, Pro, Met, His, Lys, Asp, Glu, Gly, Ala, Leu were added sequentially into Elisa plate, then, added 100 µl of buffer (pH 4.0, 0.2 M), 10 µl of Fe-MoS_2 (0.2 µg/ml concentration of $FeMoS_2$), 50 µl of

TMB (600 μM), and 50 μl of H_2O_2 (400 μM) to the above given solutions. Photographs and UV–Vis spectra were recorded after 15 min incubations at room temperature (RT).

3.2.5 Optimization of the analytical parameters

The effect of pH from 2 to 10 of the solution on the color response of Fe-MoS_2 and GSH was tested by using buffer solutions of different pH, and an optimal color was obtained at pH (Figure 3.7). The solution color was affected at lower (pH 2) as well as at higher pH.

3.3 RESULTS AND DISCUSSION

3.3.1 Nanomaterials Synthesis and their characterizations

The morphological studies of the synthesized samples were done by SEM. Figure 3.1 (a,b) is depicting that the pure MoS_2 shows a compact aggregated flower-like morphology, consisting of interweaved MoS_2 nanosheets while Fe-MoS_2 displays a petal-like morphology rather than flower-type morphology, hence, Fe-MoS_2 have a greater surface area and provide highly exposed active sites for sensing purposes. The SEM characterization shows that percentage Fe-doping can alter the shape and size of MoS_2. Further the EDS mapping has been done as shown in Figure 3.2 which clearly signifies uniform distribution of Fe in MoS_2 lattice. Figure 3.3 shows the EDS spectrum designating the existence of Fe, Mo, and S in the material. Similarly, TEM (FEI, TECHNAI G^2 20 TWIN; Czech Republic) analysis suggests a difference in interlayer spacing of MoS_2 Figure 3.1 (c,d), Fe-MoS_2 Figure 3.1 (e,f). TEM images of Fe-MoS_2 show that the interlayer spacing decreases upon doping of MoS_2 with Fe. The interlayer spacing is 0.621 nm, as well as 0.610 nm for MoS_2 and Fe-MoS_2, respectively. Well-defined rings in the SAED pattern confirm the polycrystalline property of MoS_2 as well as Fe-MoS_2. The functional group investigation has been done using FTIR as shown in Figure 3.1 (g). In case of Fe-MoS_2, the peaks at 597, 746, 1125, 1413, 1650 cm^{-1} are attributed to MoS_2 while peak at 454 cm^{-1} can be due to Mo-S stretching vibrational mode. Broad peak at

3355 cm^{-1} signifies the OH stretching vibration. Similar peaks could be observed in case of MoS_2 with slight shift in vibrational frequency [Feng et al., 2015; Lalithambika et al., 2019].

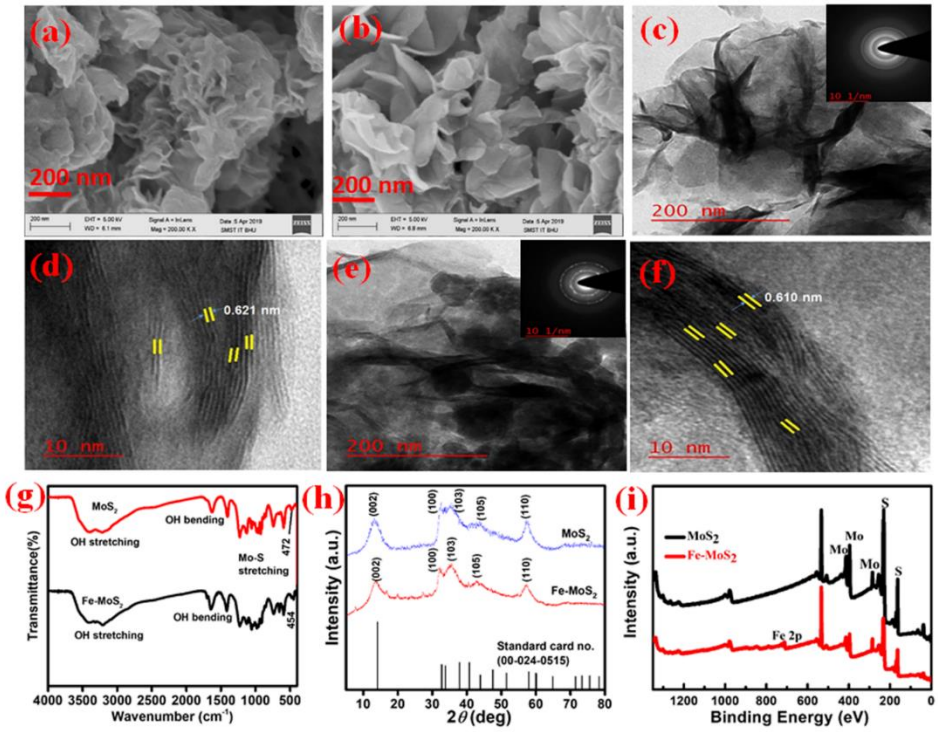

Figure 3.1 SEM images for (a) Pure MoS_2 (b) Fe-MoS_2. TEM images for MoS_2 (c,d) and Fe-MoS_2 (e,f). Analogous SAED (selected area electron diffraction) for MoS_2 (inset c) and Fe-MoS_2 (inset e), (g) FTIR spectra for MoS_2 and Fe-MoS_2. XRD profiles of MoS_2 as well as Fe-MoS_2 (h). XPS survey spectrum of pristine MoS_2 and Fe-MoS_2 (i).

The microstructures of synthesized nanomaterials were determined by powder XRD. And as per observations in Figure 3.1 (h), the MoS_2 and Fe-MoS_2 have five poor diffraction peaks at around 2θ = 13.5°, 32.4°, 34.8°, 42.8° and 57.5°, which is indexed by the (002), (103), (100), (110) and (105) planes of 2*H*–MoS_2 (JCPDS: 39-1492) [Massey et al., 2016]. Based on this, we may conclude that iron atoms are occupying a position similar of Molybdenum in a lattice of Fe-MoS_2. As the intensity of the (002) plane is higher in the case of Fe-MoS_2, it is a clear indication of higher crystallinity as well as the number of stacked layers in Fe-MoS_2 compared

to Pure MoS_2. The glass peak comes near 25° indicated by an asterisk sign (*) (The peak appears as we were preparing the sample by drop-casting on a small piece of glass slide).

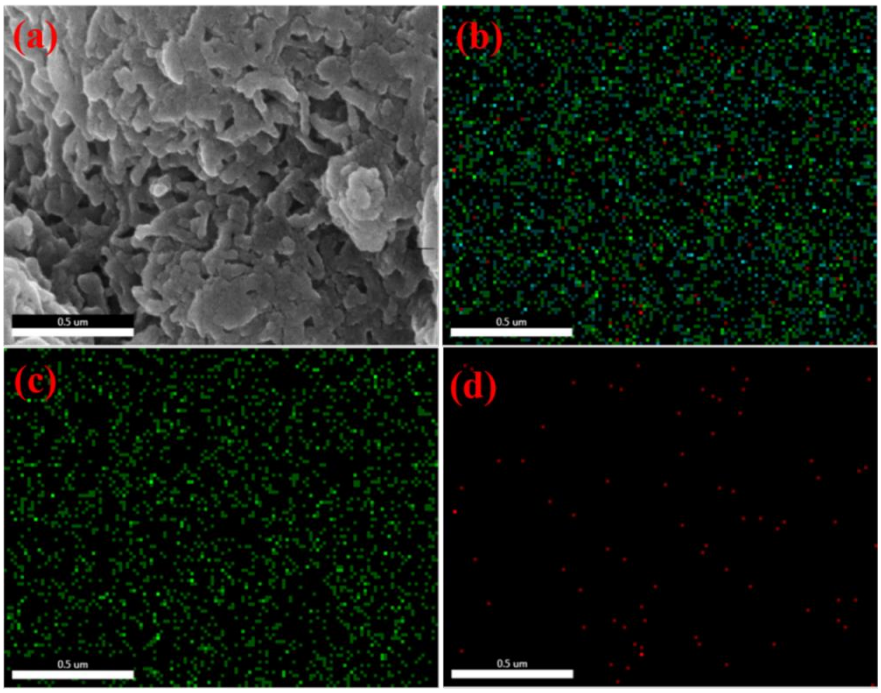

Figure 3.2 EDS mapping. (a) SEM image for mapping, (b) Elemental mapping of Mo, (c) S, (d) Fe

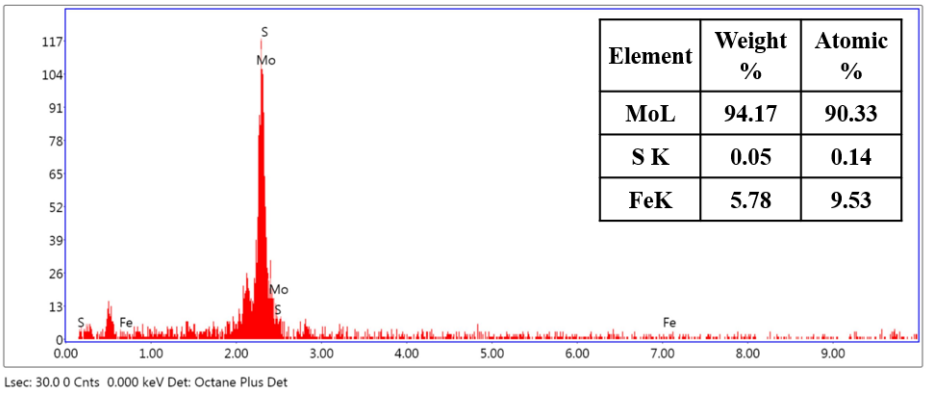

Element	Weight %	Atomic %
MoL	94.17	90.33
S K	0.05	0.14
FeK	5.78	9.53

Figure 3.3 EDS spectrum of Fe-MoS_2

XPS survey spectra were used to study the elemental composition of hydrothermally synthesized Fe-MoS_2 as well as pure MoS_2 (Figure 3.1 (i)). For the high-resolved XPS of Fe-MoS_2 sample, we are getting six peaks in the Mo 3d region while we are getting five peaks for pure MoS_2. The additional peak was observed corresponding to Fe in Fe-MoS_2. In Fe-MoS_2, the peak at 226.8 eV is related to S 2s of MoS_2 and major peaks at 229.6 eV and 232.8 eV correspond to Mo(IV) $3d_{5/2}$ and Mo(IV) $3d_{3/2}$ binding energies, respectively. Minor peaks corresponding to Mo(VI) at 233.8 eV (Mo $3d_{5/2}$) and 236.8 eV (Mo $3d_{3/2}$) indicate partial oxidation of Mo(IV) to Mo(VI) during hydrothermal synthesis [Zhao et al., 2017]. A shoulder peak is also observed at 230.7 eV for partial oxidation of Mo(IV) to Mo(V). From figure 3.4 (c) for S 2p, we are getting three peaks at 163.1 eV and 164.5 eV marked as S $2p_{1/2}$ and S $2p_{3/2}$, while the other peak at 161.7 eV attributed to the S $2p_{3/2}$ [Ojha et al., 2020].

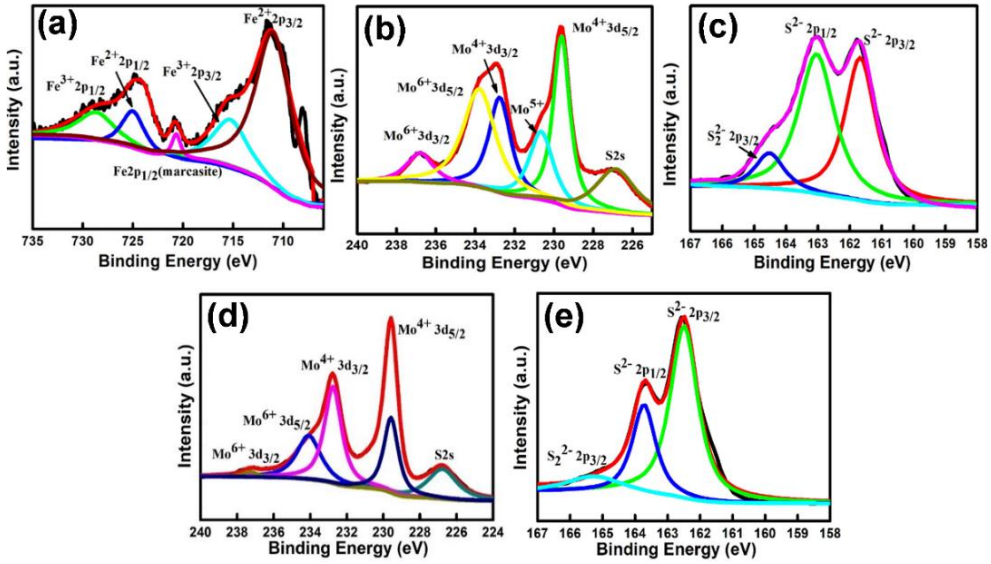

Figure 3.4 XPS spectra of Fe-MoS_2 corresponding to (a) Fe 2p, (b) Mo 3d, (c) S 2p. XPS spectra of MoS_2 (d) Mo 3d, (f) S 2p.

Deconvoluted Fe 2p XPS spectrum is shown in Figure 3.4 (a) where we are getting foremost a peak at 711.10 eV for Fe $2p_{3/2}$ and 725.06 eV for Fe $2p_{1/2}$ of Fe^{2+} species [Yamashita et al., 2008]. The difference is due to the Fe-doping into the MoS_2 sheets. The peak at 711.10 eV (Fe

$2p_{3/2}$) is shifted to 715.37 eV and other peaks 725.06 (Fe $2p_{1/2}$) is shifted to 728.73 eV which suggest an interaction between MoS_2 and Fe as our proposed materials. The marcasite peak appeared at 720.67 eV (Fe $2p_{1/2}$,) which is very common and finger mark for Fe species.

3.3.2 Choice of materials

Lots of materials such as platinum and gold nanoparticles, carbon nitride nanocomposites, MoS_2 nanosheets, vanadium disulfide nanosheets, etc. exhibits peroxidase-like activity [Tan et al., 2017]. Still, there is a significant loss of noble metals during its application in sensing because of the accomplishments of noble metal nanoparticles in a disposable way [Ni et al., 2018; Zhao et al., 2015]. Also, due to high costs, uncontrolled aggregation, sponginess and thermal stability of various nanozymes, their hands-on applications are restricted. So, the unchanging surface of non-noble metal-doped transition metal dichalcogenides can produce biomimetic active centers.

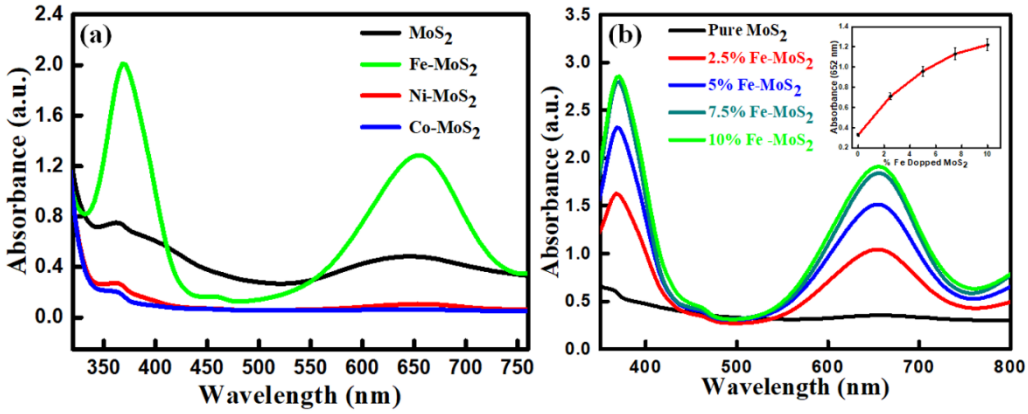

Figure 3.5 (a) UV-Visible spectrum representing comparison for mimetic behavior of various metal ions decorated MoS_2. (b) UV-Visible Spectrum and (inset b) Endpoint spectrum at 652 nm showing the effect of percentage doping of Iron on the mimetic activity of MoS_2.

Hence, different non-noble metals (Fe, Ni, Co) doped MoS_2 are tested for showing mimetic activity and among these Fe-MoS_2 has attracted immense attention due to its low-cost, high catalytic activity, high thermal and chemical stability. Further, we have

tested the enhancement in mimetic activity of our material using different doping concentrations of Fe (i.e. 0, 2.5, 5, 7.5, 10%). Finally, a good platform is produced for the detection of GSH using Fe-MoS_2 as more enzymes are entangled in flower-like structures to raise its mimetic activity. We have used the outstanding catalytic (mimetic) activity of Fe-MoS_2 for optical GSH sensing.

3.3.3 Peroxidase mimetic behavior for Fe-MoS_2 and colorimetric probe for GSH detection

The chromogenic substrates TMB is used to display the peroxidase activity of Fe-MoS_2 [Nirala et al., 2015]. As displayed in Figure 3.5 (a), TMB oxidation by Fe-MoS_2 using H_2O_2 is catalyzed to give a blue-colored compound (oxTMB) with an absorbance value of 652 nm. Among various doped MoS_2 as well as Pure MoS_2, Fe-MoS_2 exhibits better performance for peroxidase-like activity. Activity is also dependent upon % doping of Fe in Fe-MoS_2 (Figure 3.5 (b)) with a saturation effect at around 10% doping. From Figure 3.6, it is shown that the intensity of absorbance peak value at 652 nm of Fe-MoS_2-TMB-H_2O_2 increases with time and has rapid catalytic behavior than Fe-MoS_2–TMB and TMB–H_2O_2 system. Hence, it is confirmed that Fe-MoS_2 shows a powerful mimetic activity of peroxidase substrates [Wen et al., 2014]. However, the TMB oxidation is quenched with the addition of some amount of GSH (Figure 3.6, curve c), followed by an acute drop in the absorbance, showing that the mimetic activity of the Fe-MoS_2 is inhibited by the presence of GSH. As reported in the literature, the adsorption of H_2O_2 molecules on the Fe-MoS_2 surface by collision leads to the breakup of O-O bond of H_2O_2 into $OH^{\cdot}$ radicals. The highly oxidative nature of $OH^{\cdot}$ radicals causes the oxidation of colorless TMB [Feng et al., 2017]. The addition of GSH to the Fe-MoS_2–TMB system results in the blue color contrast (curve c, Figure 3.6).

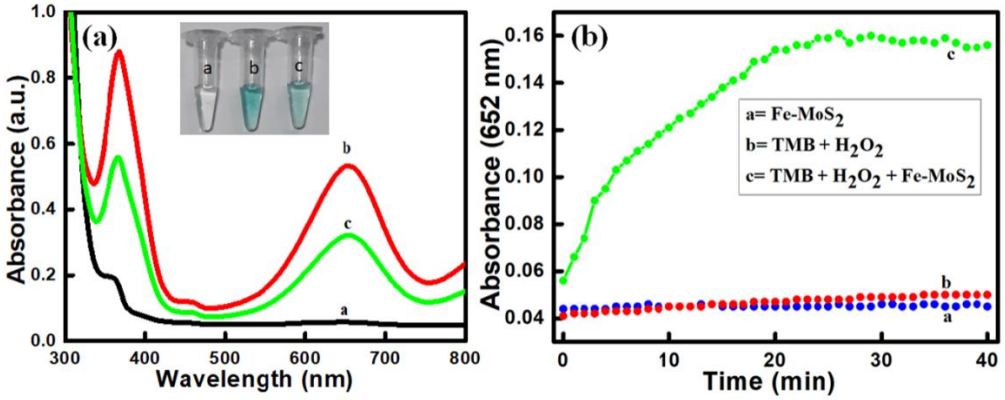

Figure 3.6 UV-Visible spectra with different combinations (a) GSH (100µL) +TMB (50µL) (b) Fe-MoS_2 (10µL) + TMB (50µL) (c) GSH (100µL) + Fe-MoS_2 (10µL) + TMB (50µL) (B) time-based kinetic study for (a) Fe-MoS_2, (b) H_2O_2+ TMB and (c) Fe-MoS_2 + H_2O_2+TMB. (corresponding contrast image shown in inset). TMB (600 µM), Fe-MoS_2 (0.2 µg/ml), and H_2O_2 (400 µM) was the corresponding concentration used in the system.

The oxidized TMB exhibits signals at the wavelength of 652 nm and 365 nm in UV-Visible spectra because of the development of a complex (charge-transfer) between unoxidized and oxidized TMB compounds resulting in a blue-colored product. Fe-MoS_2-TMB-H_2O_2 pattern is used for the GSH detection corresponding to differing in absorbance value at 652 nm with different concentrations of GSH.

3.3.4 Temperature and pH-dependent peroxidase mimetic activity of Fe-MoS_2

The role of different physical parameters such as pH and temperature on the catalytic activity of Fe-MoS_2 has been considered (Figure 3.7). The pH and temperature (above 60 °C) have an adverse effect on the catalytic activity of the natural enzymes. Fe-MoS_2 exhibits good and stable catalytic activity throughout a long-range of temperature and pH (Figure 3.7 (a,b)) in comparison to natural enzyme HRP [Lin et al., 2014]. Fe-MoS_2 was found to exhibit optimum mimetic activity in a slightly acidic environment (pH 4.0) in

comparison to other peroxidases. The wide range of physical factors like pH and temperature would be beneficial for sensing applications.

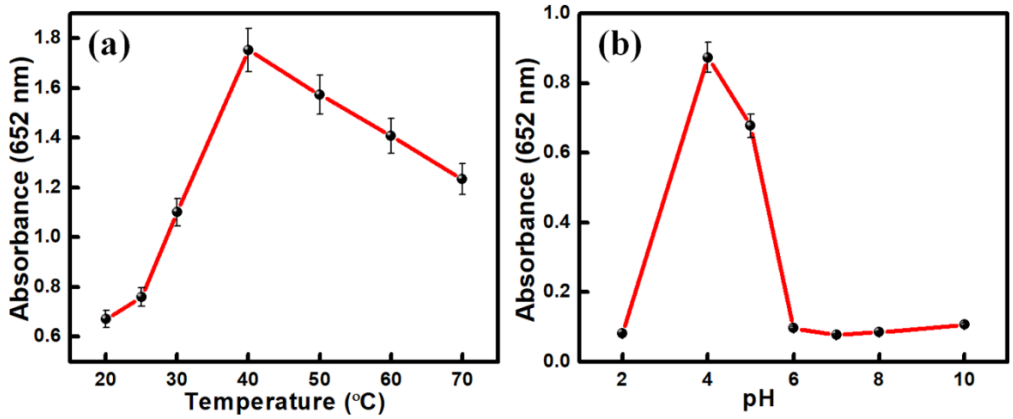

Figure 3.7 The catalytic behaviour of Fe-MoS_2 dependent of (a) Temperature, (b) pH. Optimized reaction condition are Fe-MoS_2 (0.2 μg/ml), TMB (600 μM), H_2O_2 (400 μM), 100 μl of acetate buffer at room temperature.

3.3.5 Kinetics study of Fe-MoS_2 flowers

The steady-state kinetics has been studied for Fe-MoS_2 for TMB and H_2O_2 by keeping the constant concentration of either TMB or H_2O_2 and varying others. The initial rate (V_0) for the peroxidase mimetic activity of Fe-MoS_2 has been calculated by utilizing the Beer–Lambert Law [Nirala et al., 2015].

$$\text{Conc.} = A/\varepsilon b \quad \ldots\ldots\ldots\ldots\ldots\ldots\text{(Eq. 3.1)}$$

Where Conc. denotes the concentration of substrate, b is the thickness of the solution, A is the absorbance. The molar absorption coefficient Ɛ of oxidized TMB product, with 39,000 $M^{-1}cm^{-1}$ value was calculated. The Michaelis–Menten equation is followed by Fe-MoS_2 using substrate TMB and H_2O_2 at suitable concentrations. The Michaelis–Menten constant (K_m) for the catalyst and maximum initial velocity (V_{max}) has been calculated from the Michaelis–Menten equation (Figure 3.8 (a,b); Eq. 3.2).

$$V_0 = \frac{V_{max}\,[S]}{K_m + [S]} \quad \text{.....(Eq. 3.2)}$$

Table 3.1 Comparative table of steady-state kinetics of different catalytic substrates through TMB oxidation.

Catalytic substrate	K_m (mM)		V_{max} (M s^{-1})		Reference
	TMB	H_2O_2	TMB	H_2O_2	
Fe-MoS_2	0.387	0.0638	9.5×10^{-6}	4.385×10^{-6}	Present work
MoS_2	0.525	0.0116	5.16×10^{-8}	4.29×10^{-8}	[Lin et al., 2014]
HRP	0.434	0.065	14.72×10^{-8}	5.65×10^{-8}	[Zheng et al., 2013]
AuNPs	0.11	61.34	15.39×10^{-9}	6.63×10^{-9}	[Xue et al., 2021]
Au@HMPB	0.25	88.72	0.34×10^{-6}	0.25×10^{-6}	[Zhou et al., 2019]
AuNPs @C_3N_4	0.097	12.3	1.52×10^{-8}	9.0×10^{-8}	[Wu et al., 2019]

Where K_m is the concentration (S) of the substrate at half of the maximum initial velocity, V_{max} stands for the maximum initial velocity. The results show lower K_m value of Fe-MoS_2 in respect to H_2O_2 and TMB than HRP and pristine MoS_2 which suggests higher affinity of Fe-MoS_2 towards TMB substrates than others. V_{max} value is found to be higher than HRP and MoS_2 which advocates better catalytic activity of Fe-MoS_2. The kinetic parameter of Fe-MoS_2 has been compared from literature (Table 3.1) with our findings that express Fe-MoS_2 has good kinetics with higher V_{max} and low K_m value over MoS_2 and natural peroxidase because of greater surface area and active sites for the binding of H_2O_2

and TMB. The results also support synergistic enhancement in catalytic activity due to iron doping.

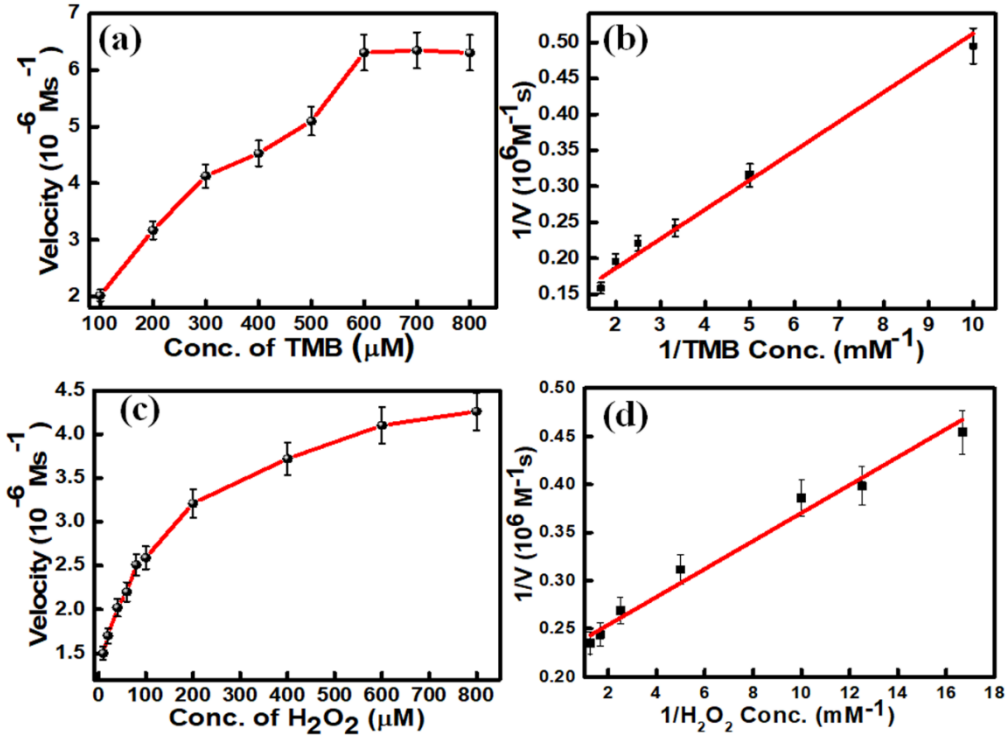

Figure 3.8 Enzyme kinetic study of Fe-MoS_2 was done. Optimized condition of Fe-MoS_2 (0.2 μg/ml) in 100 μl of acetate buffer (A,B) Kinetic study of Fe-MoS_2 for TMB in a constant H_2O_2concentration (400 μM) (C,D) kinetic for H_2O_2 in constant TMB concentration (600 μM).

3.3.6 Colorimetric detection of GSH

As evident by SEM image, it can be inferenced that on doping MoS_2 with Fe, the morphology of the MoS_2 changes from flower like to petal like with relatively larger surface area. MoS_2 have intrinsic peroxidase activity and oxidizes TMB in presence of H_2O_2, but on doping with Fe, the peroxidase activity is significantly enhanced that may be due to increase in the catalytic surface area of nanozyme. The catalytic oxidation of TMB results in generation of blue color product (charge transfer complex with characteristic absorption maxima at 652 nm). On introduction of the GSH, the OH radical produced as a

result of peroxidase activity of Fe-MoS_2, oxidizes GSH to GSSH and thereby inhibiting the oxidation of TMB. Thus, with increase in GSH concentration, we get a decrease in absorption intensity at 652 nm with a clear blue color contrast as shown in Figure 3.9.

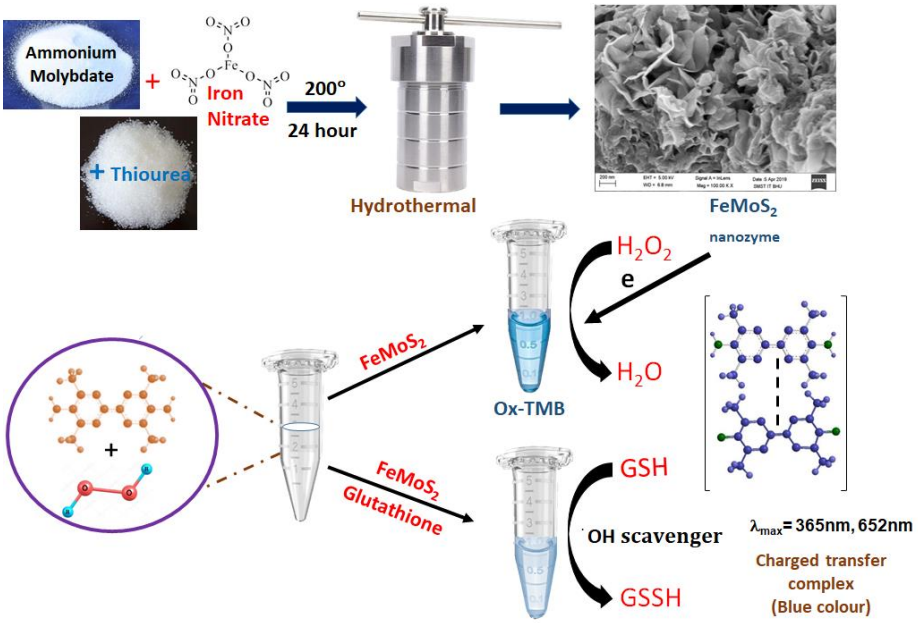

Figure 3.9 The proposed mechanism for the GSH detection through colorimetric method based on TMB oxidation in the presence of H_2O_2 and catalytically active Fe-MoS_2.

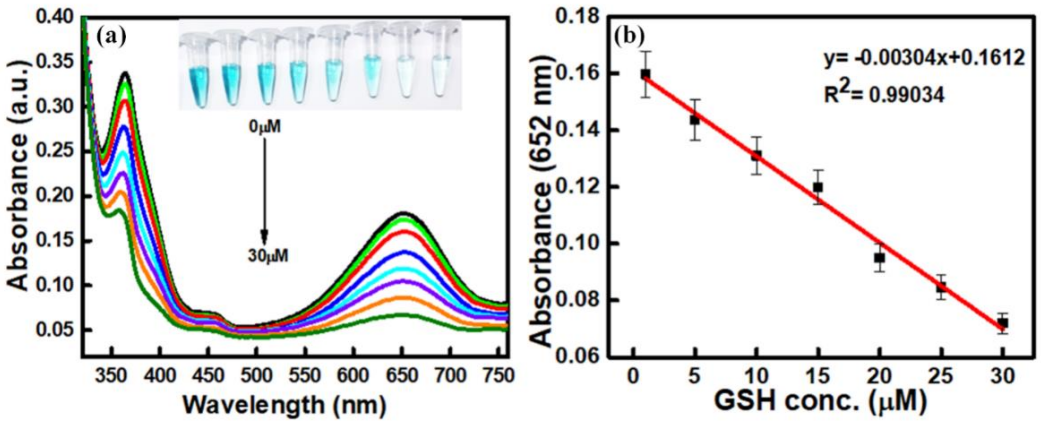

Figure 3.10 (a) UV-Visible spectra for colorimetric (optical) sensing of GSH in acetate buffer based on Fe-MoS_2 + TMB + GSH. Inset shows color change with varying GSH concentration (0, 1, 5, 10, 15, 20, 25, 30μM) (b) curve for calibration plot.

Figure 3.10 shows a decrease in the absorbance intensity with an increase in GSH concentrations in the developed sensing system. The developed sensor exhibited good linear response in the region 1-30 μM with a better limit of detection (0.577 μM) calculated by using formula 3σ/slope by calibration plot (Figure 3.10 (b)) paralleled to GSH detection established on numerous substrates described in the literature. On behalf of the comparison table, it states that the Fe-MoS_2 system is cost- effective as well as has better catalytic activity in comparison to others. (Table 3.2)

Table 3.2 Comparison of various nanoparticles-based methods for detection of GSH

S.N.	Substrate	Method	LOD	Linear range	Remark	Ref.
1	Fe-doped MoS_2	Colorimetry	0.577 μM	1-30 μM	Cost-effective	This work
2	Ag+	Colorimetry	0.1 μM	0.05-8 μM	Costly	[Ni et al., 2014]
3	Gold nanocluster	Colorimetry	0.420 μM	2-25 μM	Costly Noble metal used	[Feng et al., 2017]
4	Lanthanide-MnO_2	Fluorometry	0.9 μM	-	-	[Deng et al., 2011]
5	Biotin-QD-MnO_2 nanocomposite	Fluorometry	16.3 μM	0.05-1.2 mM	-	[Chen et al., 2018]
6	Citrate capped AuNPs	Colorimetry	3.3 μM	1-100 μM	Costly	-N [Hormozi ezhad et al., 2012]

(Costly means expensive or high cost. Cost-effective means are profitable/ worthwhile)

3.3.7 Interfering study

The developed sensor shows selectivity towards GSH detection based on Fe-MoS_2 has been studied by using an essential methodology known as Interference study. First, the concentration GSH is fixed and various interferences from numerous amino acids consisting of Ala, Gly, Leu, Try, Asp, Pro, His, Met, Lys, Glu with the concentration of

1mM (10 times higher) and also interferences with mercapto groups like Cys and Hcys have been studied. The concentration of Cys, Hcys and GSH was taken as 100 μM. The results proposed that the change in absorbance at 652 nm for GSH is comparable while other interferences have a negligible effect on the colorimetric GSH sensor (Figure 3.11). The developed method also exhibits good selectivity towards GSH over other mercapto molecules. The result suggests that Fe-MoS_2 is a better candidate for the development of the GSH sensor.

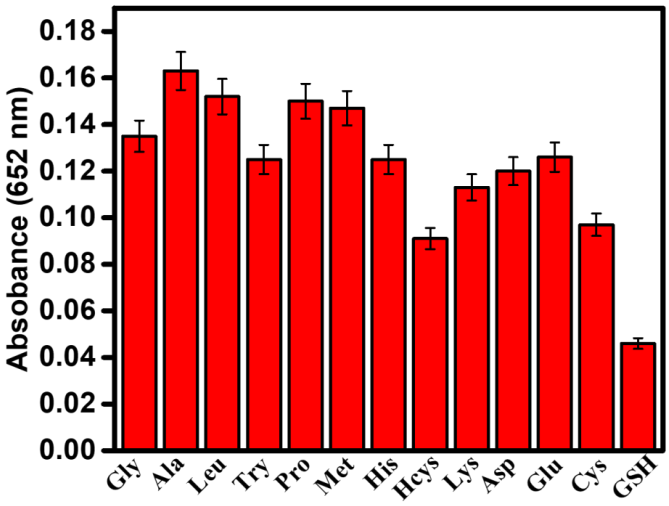

Figure 3.11 Interference study of GSH with different amino acids. Reaction condition like 100 μL of sodium acetate buffer with TMB (600 μM), 0.2 μg/ml Fe-MoS_2 and 400 μM H_2O_2 with different interference.

3.3.8 Durability and recyclability study

The experimental results have been further validated by studying the reproducibility of the developed sensor. Both inter-day (1-4 days) and intra-day (0-12 hours) experiments were performed for studying repeatability under identical experimental environments for detection of GSH (0μM to 30 μM) depicted in (Figure 3.12 (a) and (b)). The obtained result suggests that the established GSH sensor based on Fe-MoS_2 is highly reproducible with excellent stability for the detection of GSH.

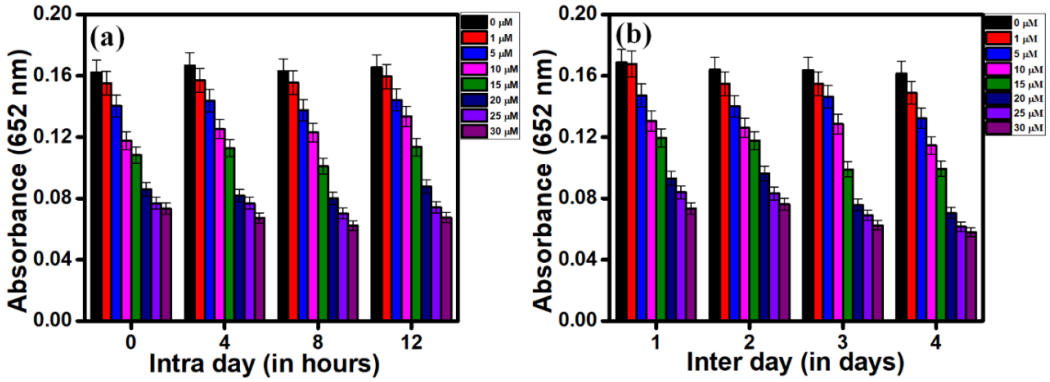

Figure 3.12 The reproducibility of the developed colorimetric sensor (a) Intra as well as (b) Inter-day research in identical conditions for GSH(0 μM to 30 μM) detection.

3.3.9 Testing the GSH level in human serum

The proposed sensing method has been further utilized to develop a sensor for the quantification of the GSH in a biological sample (serum). In a healthy person, a normal range of GSH in serum is 2-5 μM but serious complications and physiological disorders when the concentration exceeds beyond the normal limit. For the GSH sensing, blood serum was diluted 30 times and stuck with different concentrations of the GSH (0, 1, 5, 10, 15, 20, 25, 30 μM). The rise in the GSH concentration in the blood serum inhibits the oxidation of TMB substrate and results in a decrease in absorbance (Figure 3.13 (a, b)).

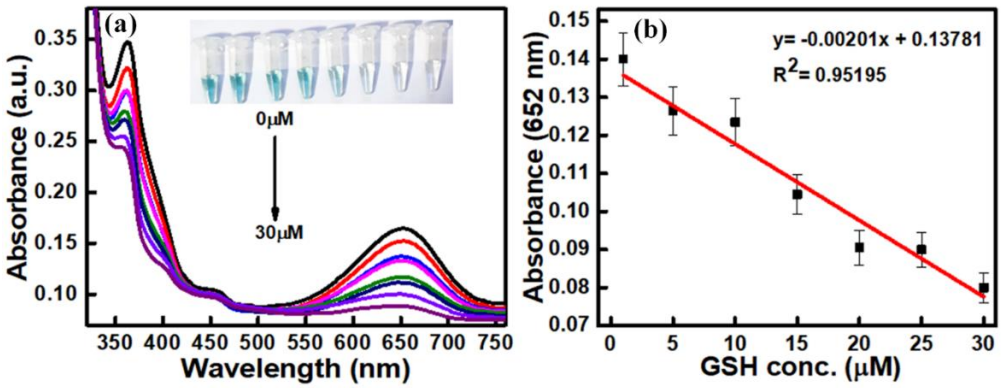

Figure 3.13 (a) UV-Visible spectrum of GSH level in the blood sample (based on Fe-MoS_2) and the color change of Eppendorf solution in presence of GSH level shown in the inset (at concentrations: 0, 1, 5, 10, 15, 20, 25, 30μM), and (b) corresponding calibration curve.

The developed sensor shows good linear response in the range 1-30 μM with regression coefficient 0.95 and limit of detection was found to be 6.06 μM.

3.4 Conclusions

In conclusion, we have economically synthesized Fe-MoS_2, which is exhibiting an excellent peroxidase mimetic activity for chromogenic peroxidase substrates (TMB) that gives blue-colored contrast in the presence of H_2O_2. The enzyme kinetics is ideally followed by the Fe-MoS_2 which is validated through Michaelis–Menten kinetics for peroxidase mimetic activity. Fe-MoS_2 promotes electron transfer for a spontaneous H_2O_2 breakdown into $OH^{\cdot}$, which causes oxidation of TMB to give the blue color product. The result shows synergistic enhancement in the catalytic activity of MoS_2 because of the doping effect. We have exploited the above nanomaterial for fruitful detection of GSH level in an acetate buffer and serum samples having outstanding sensitivity and selectivity. The advanced colorimetric technique based on Fe-MoS_2 as peroxidase mimics can be beneficial in the field of clinical diagnosis.